Ground-based prototype quantum cascade laser heterodyne radiometer for atmospheric studies

D. Weidmann, W. J. Reburn, and K. M. Smith
STFC Rutherford Appleton Laboratory, Space Science and Technology Department, Didcot, Oxfordshire, OX11 0QX, United Kingdom

(Received 10 January 2007; accepted 7 June 2007; published online 27 July 2007)

The advent of quantum cascade lasers has provided matured continuously tunable solid state laser sources emitting from mid-infrared to terahertz wavelengths. Such sources, used as local oscillators, offer the practical prospect of aircraft, high altitude platform, and satellite deployment of compact and shot noise limited heterodyne radiometers for Earth observation and astronomy. A ground-based prototype of a quantum cascade laser heterodyne radiometer operating in the mid-infrared has been developed and is presented. The instrument design and concepts are described, together with evaluation of the instrument in the laboratory and during field measurements of atmospheric ozone. In this study the best performance achieved by the prototype quantum cascade laser heterodyne radiometer was a signal-to-noise ratio of three times the theoretical shot-noise limit. The prototype has allowed the main sources of excess noise to be identified as residual optical feedback in the local oscillator optical path and a lack of mechanical and thermal stability in the local oscillator collimation system. Instrument improvements are currently being implemented and enhanced performance is expected in the near future. © *2007 American Institute of Physics.*
[DOI: 10.1063/1.2753141]

I. INTRODUCTION

Since the pioneering work of Teich *et al.*,[1] infrared (IR) laser heterodyne techniques have been successfully used for the last 40 years in the field of remote sensing, for both atmospheric sciences and astronomy.

As far as atmospheric (here "atmospheric" applies to studies of the Earth atmosphere; studies of planetary atmospheres is considered to be more in the remit of astronomy) applications are concerned, seminal works were undertaken by Menzies and Shumate[2] and Menzies.[3] Since then, laser heterodyne radiometers have been extensively used for the studies of stratospheric species like ozone (see, for example, the most recent work reported by Fast *et al.*[4]) or $ClONO_2$,[5] primarily because of their ultrahigh spectral resolution measurement capability. On the other hand, in the field of astronomy, heterodyne spectro-radiometry has been highly successful and the most impressive results have been obtained, for example, with the instrument from the NASA Goddard Space Flight Center,[6] in detecting the spectral features of gases in planetary atmospheres,[7] in measuring local gas velocities,[8] or even in detecting naturally occurring stimulated emission in the Martian atmosphere.[9]

Infrared heterodyne techniques have also been successfully employed for optical stellar interferometry, the Infrared Spatial Interferometer operating at Mount Wilson being a unique example.[10]

Most of the work cited above has been performed using CO_2 gas lasers as the local oscillator source. Alternative approaches using lead salt lasers have been investigated, the latest developments being reported in Refs. 11 and 12. However, these lasers have been shown to have serious drawbacks that impede their use in "real-world" IR heterodyne applications. The advent of mid-infrared quantum cascade lasers[13] (QCLs) offered a serious alternative to the use of lead salt lasers, as QCLs offer the prospect of room-temperature operation[14] coupled with a wide spectral tuning range through external-cavity operation.[15] Their long lifetime, compactness, and robustness are advantages which also make them suited to flight and space qualification. The use of QCLs as local oscillator has been evaluated by Sonnabend *et al.*[16] Following the evaluation, an instrument has been developed for astronomy applications[17] and has successfully demonstrated observations of planetary atmospheres.[18]

This article presents the development of a QCL-based mid-IR heterodyne spectro-radiometer [referred to hereafter as the laser heterodyne radiometer (LHR)]. This ground-based prototype LHR is dedicated to the evaluation of the technique for heterodyne radiometry from space, primarily, but not exclusively, for Earth observation. Atmospheric ozone has been chosen as the target compound to demonstrate the prototype, because of its important role in both stratospheric and tropospheric chemistry and its impact on air quality. Ozone, especially that present in the stratosphere, has already been investigated with heterodyne systems [e.g., Refs. 19–22], since these instruments provide the high spectral resolution required to resolve true line shapes at low pressures when only Doppler broadening occurs. From space high spectral resolution is required to observe tropospheric ozone since at low resolution the strong stratospheric contribution will obscure the tropospheric component, which is about two orders of magnitude smaller and has a very small temperature contrast with the ground (~ -5 K/km gradient).

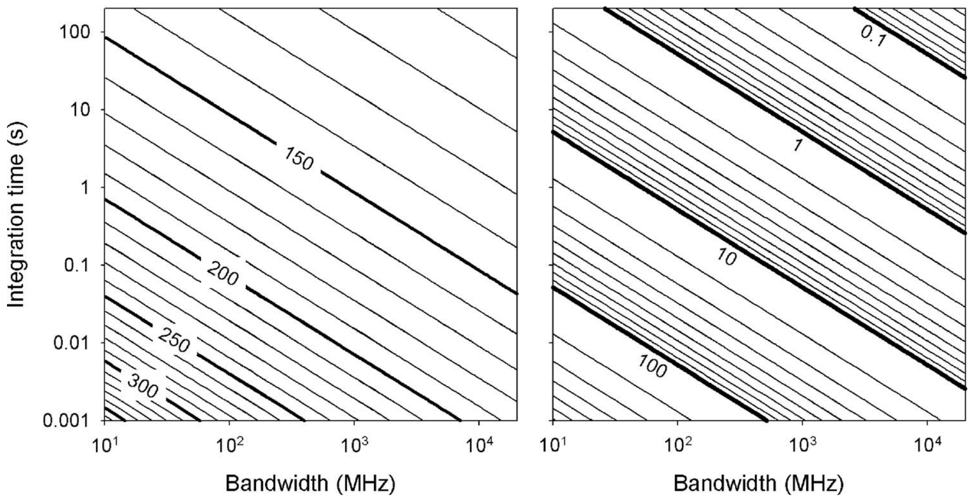

FIG. 1. The minimum detectable brightness temperature difference (left) and the noise equivalent radiometric sensitivity (right) for a shot-noise limited infrared heterodyne radiometer operating at 10 μm with a 50% heterodyne efficiency. Figures appearing in the contour plots are in Kelvin.

Knowledge of the stratospheric contribution to the total ozone signal is therefore required before it is possible to retrieve the tropospheric component.

This article is organized as follows: the first part is an introduction to infrared heterodyne instruments and the second section deals with the characteristics of QCLs and their use as tunable local oscillators. In the next two parts, the instrument design is presented and discussed followed by results obtained both in the laboratory and during an atmospheric measurement campaign.

II. LASER HETERODYNE RADIOMETRY IN THE MID-IR

The heterodyne technique down-converts a received signal to a lower frequency, usually referred to as the intermediate frequency (IF) signal, which can be processed more easily. This is achieved by mixing incident radiation with that from a local oscillator at a detector with a nonlinear response (see Ref. 3 for more details). The IF signal can be divided and amplified without degradation of the signal-to-noise ratio (SNR), allowing efficient spectral multiplexing. The advantages and specificities of IR laser heterodyne detection are discussed below.

A. Sensitivity

Heterodyne instruments are well developed for spectroradiometry in the radio and microwave regions, as in this part of the spectrum direct detection systems are not practical. Heterodyne instruments provide both spectral and radiometric information about the incident radiation. Hereafter these instruments are referred to as radiometers, but one should keep in mind that they are also excellent spectrometers. An ideal shot-noise limited heterodyne radiometer exhibits detector noise of one photon per second per unit of bandwidth. Consequently the noise limit scales with photon frequency, and therefore it increases from the radio to the optical regions of the spectrum. The noise equivalent power (NEP) for an ideal heterodyne radiometer is given by the Eq. (1),[3] where η is the heterodyne efficiency, h is the Planck constant, ν is the frequency, B is the receiver bandwidth, and τ is the integration time. Equation (1) only takes into account the shot noise induced by the local oscillator. When the LO power is milliwatts or above, shot noise and excess noise from the signal source and from the background, as well as Johnson noise, can be neglected.

$$\mathrm{NEP} = \frac{h\nu}{\eta}\sqrt{\frac{B}{\tau}}. \tag{1}$$

The power received by the ideal heterodyne radiometer from a blackbody source at temperature T is expressed by

$$P = \frac{1}{2} I(\nu,T)\lambda^2 B, \tag{2}$$

where $I(\nu,T)$ is the Planck equation. The factor of one-half allows for the radiometer's sensitivity to polarization, and λ^2 is the throughput of a single spatial mode. From Eqs. (1) and (2), the minimum brightness temperature difference the radiometer can detect is

$$T_{\min} = \frac{h\nu}{k \log(\eta\sqrt{B\tau}+1)}. \tag{3}$$

It is worth noting that the Rayleigh-Jeans approximation is not valid in the mid-infrared; however, at microwave frequencies where the Rayleigh-Jeans approximation is valid, Eq. (3) becomes equivalent to the usual noise temperature equation for microwave heterodyne systems (e.g., Ref. 23).

A trade-off has to be found between B and τ, between spectral resolution and acquisition speed, since B also defines the resolution of the instrument. Figure 1 shows contour plots of the minimum detectable temperature difference (left panel) and the noise equivalent radiometric sensitivity (right panel) as a function of both the radiometer receiving bandwidth and the integration time. These plots were generated for a shot-noise limited heterodyne radiometer operating at 10 μm, with a 50% photomixer heterodyne efficiency. The radiometric sensitivity ΔT was defined from the signal-to-noise ratio $\mathrm{SNR_{HET}}$, such that:

$$\frac{P}{\Delta P} = \mathrm{SNR_{HET}}. \tag{4}$$

B. Comparison with Fourier transform spectrometers

It is interesting to briefly compare heterodyne radiometry with Fourier transform spectrometry, since the latter is widely used for high-resolution radiometry in the thermal infrared. The SNR of a Fourier transform spectrometer (FTS) is discussed in Ref. 24,

$$\mathrm{SNR}_{\mathrm{FTS}} = I(\nu,T)U\xi\Delta\nu D^{*}\sqrt{\tau}(A_D)^{1/2}, \tag{5}$$

where U is the FTS throughput, ξ is the efficiency, $\Delta\nu$ is the resolution, D^* is the detector detectivity, and A_D is the physical area of the detector element. Note that the Eq. (5) only considers the detector noise. It follows that

$$\frac{\mathrm{SNR}_{\mathrm{HET}}}{\mathrm{SNR}_{\mathrm{FTS}}} = \frac{c^2}{2h}\frac{\sqrt{A_D}}{U\xi D^{*}}\eta\frac{1}{\nu^3\sqrt{\Delta\nu}}. \tag{6}$$

The right hand side of Eq. (6) has been organized into specific terms. The first term is a constant. The second term is related to the performance of the FTS. The last term shows that heterodyne radiometry is more favorable at smaller frequencies and higher resolution. For example, considering the specifications of a typical commercially available high-resolution FTS operating at a wavelength of 10 μm, $A_D = 1$ mm^2, $U = 0.01$ cm^2 sr, $\xi = 0.1$, and $D^* = 8\times 10^{10}$ cm $\sqrt{\mathrm{Hz}}$ W^{-1}, and considering an ideal heterodyne radiometer with 50% heterodyne efficiency, Eq. (6) shows that the heterodyne radiometer has a superior SNR at spectral resolutions below 250 MHz. Of course for a given beam splitter and detector the spectral coverage of the FTS is around 500 times wider than the LHR, but as will be discussed later, the prototype LHR instrument has a footprint 15 times smaller than a typical high-resolution FTS and the maximum spectral resolution of LHR is superior to that achievable by most FTS instruments.

C. Spectral resolution

In the thermal infrared heterodyne systems offer the highest spectral resolution (up to $\lambda/\Delta\lambda = 10^7$) of any type of radiometer. The resolution is defined by electronic filtering rather than optical properties. This is a very flexible system; filters may be easily changed to suit the resolution requirements of particular measurements, and there are no additional optical components. In radiometric systems that use direct detection, optical filters and other associated optical components radiate and contribute significantly to the background radiation signal.

For atmospheric or astronomy applications where linewidths are Doppler limited a sub-Doppler resolution is required to allow accurate measurement of line shapes. High resolution combined with high frequency precision permits the precise measurement of Doppler shifts and the retrieval of gas velocity information.

Spectral resolutions of a few megahertz are achievable in the mid-IR range. As reported in Ref. 10, at such high resolutions direct detection methods are limited by nonfundamental noise (current leakage and radiation leakage). Conversely heterodyne detection is not impeded by nonfundamental noise limits as the resolution increases.

D. Field of view

In a heterodyne system the detected signal is in a single spatial mode. The throughput is limited by the operating wavelength. Using the small angle approximation, the field of view (FoV) of a heterodyne system can be expressed as:

$$\mathrm{FoV} = \frac{4\lambda}{\pi D}, \tag{6'}$$

where D is the diameter of the collecting optics. For example, an instrument with a 250 mm diameter mirror collecting radiation at 10 μm would have a FoV of ~50 μrad. This is far smaller than the FoV of conventional direct detection systems currently used for Earth observation [for comparison the LHR would have a footprint of 0.04×0.04 km^2 from a 800 km polar orbit whereas existing high spectral resolution instruments exhibit a footprint of 3×30 km^2 for the Michelson Interferometer for Passive Atmospheric Sounding (MIPAS) and 0.5×5 km^2 for the Tropospheric Emission Spectrometer (TES)]. Such a small FoV would be advantageous for monitoring localized phenomena (e.g., sources of anthropogenic or natural emissions) and increasing the number of useful observations between scattered clouds.

E. Frequency accuracy

The frequencies contained within the IF signal are directly related to the local oscillator frequency. The determination of absolute frequencies is limited by the stability of the LO frequency and how accurately and precisely the LO frequency is known. A frequency determination of better than ten parts per trillion is possible with actively stabilized lasers, and this enables the accurate and precise determination of Doppler shifts.

In conclusion to this first section, the strength of IR heterodyne radiometry is the combination of high sensitivity, small FoV, and high spectral resolution. These attributes are complimentary to other systems able to perform on a more global scale, both spatially and spectrally.

III. TUNABLE LOCAL OSCILLATOR

The ideal LO is a pure harmonic oscillator. In the optical thermal infrared region gas lasers, especially CO_2 lasers, provide the best approximation to an ideal monochromatic source. They exhibit very low levels of excess noise, excellent beam quality, and good spectral purity. Semiconductor-based laser sources have been used, namely, lead salt diode lasers. References 25 and 26 report on recent work using lead salt lasers as LOs in heterodyne systems. The move towards these devices was mainly motivated by the opening of new spectral windows not readily accessible with gas lasers, which are bound to emit radiation at wavelengths determined by particular molecular transitions. Investigations with lead salt lasers at wavelengths up to 30 μm were undertaken with astronomical applications in mind.[27] However, lead salt lasers suffer from problems such as multimode emission, low output power, and frequency variations arising from thermal cycling and aging. These drawbacks have prevented their use in real-world applications.

QCLs, first demonstrated in 1994,[13] have quickly superseded lead salt lasers in becoming reliable mid-IR continuously tunable laser sources. These devices provide high optical power (several milliwatts), single mode operation through the integration of distributed Bragg gratings, high spectral purity (in the megahertz range), and continuous tunability within 1% of the central wavelength. Potentially these qualities make QCLs ideal LOs for mid-IR heterodyne receivers.

A. Optimum wavelength selection

Atmospheric ozone was chosen as the target species to demonstrate the QCL-based LHR reported here. Useful atmospheric measurements of trace gas species are limited to so-called atmospheric transmission windows, where absorption from abundant infrared-active species such as water vapor and CO_2 is at its minimum. Inspection of the windows 3–5 and 8–12 μm indicates that the most favorable wavelength in performing ozone spectro-radiometry in the thermal infrared is the ν_3 rovibrational band centered at $\sim$1040 cm^{-1}. At these frequencies the expected tuning range of a QCL is around 10 cm^{-1}, which defines the wavelength coverage of the heterodyne spectro-radiometer. The precise wavelength selection for an ideal LHR operating in the emission mode was based on the following assumptions:

– a maximum tuning range 3 cm^{-1} wide,
– a shot-noise limited performance with 50% heterodyne efficiency,
– a ground-based zenith viewing configuration,
– a standard mid-latitude daytime atmosphere, and
– 1 s integration time.

Atmospheric simulations were run using a two-dimensional forward model;[28] a maximum-likelihood retrieval algorithm based on the Bayesian approach to the inverse problem[29] was used to determine the sensitivity of the instrument to ozone. Figure 2 shows the predicted error in the retrieved ozone concentration profile (upper plots) and the altitude resolution (lower plots) as a function of wave number and altitude. Calculations were performed for two spectral resolutions: 10 MHz and 1.4 GHz. For tropospheric ozone a concentration retrieval error of below 5% can be obtained by working either at 1030 or 1050 cm^{-1}. As one might expect, at these frequencies higher spectral resolution yields much more information on stratospheric ozone. The error in retrieved ozone concentration and the profile vertical resolution are significantly enhanced.

Laser specifications were based on the results of the simulated atmospheric retrievals, and a continuous-wave liquid-nitrogen cooled distributed feedback QCL was provided by Alpes Lasers SA accordingly. This particular laser has been fully characterized and its performance has been discussed in detail in Ref. 30. Briefly, the laser is tunable between 1030 and 1037 cm^{-1}, delivers an output power up to 35 mW, and operates single mode with a side-mode suppression ratio of better than 30 dB. Average frequency tuning rates were measured to be -3.9 cm^{-1} A^{-1} and -0.065 cm^{-1} K^{-1}.

B. Local oscillator frequency sweeping

An important feature of QCLs is their ability to be continuously tuned in frequency, and this has been widely exploited for absorption spectroscopy. In the LHR this continuous tuning is used to sweep the frequency of the LO. This method is slightly different to the one usually used in millimeter wave receiver, as rather than using filter banks, autocorrelators, or acousto-optical spectrometers, the LHR uses the continuous tuning of the LO to perform the spectral analysis. This method avoids the need for any IF signal analysis.

The spectral coverage of a heterodyne receiver is determined by the LO frequency and the electrical bandwidth of

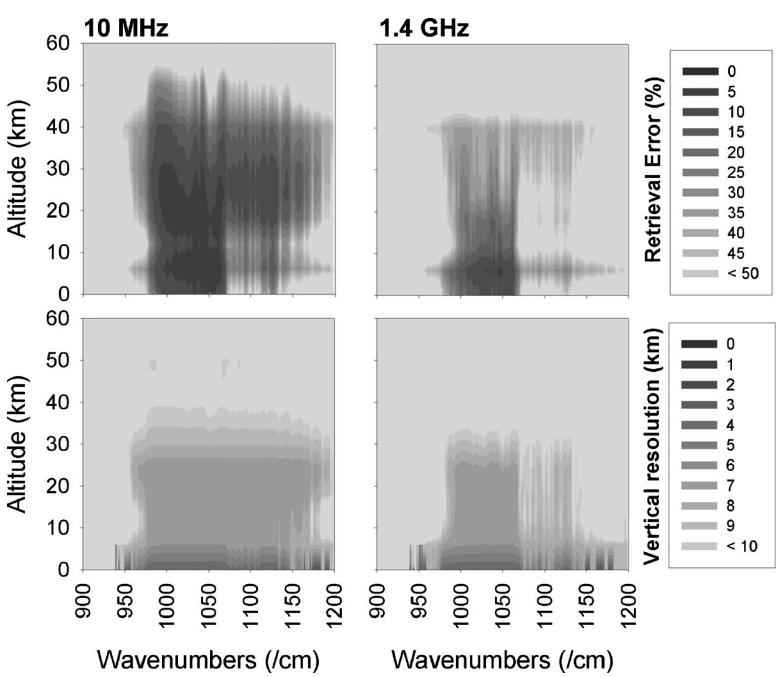

FIG. 2. Theoretical calculations of atmospheric ozone profile retrieval error (upper) and vertical resolution (lower) for an ideal infrared heterodyne receiver. Calculations were performed for two resolutions: 10 MHz and 1.4 GHz.

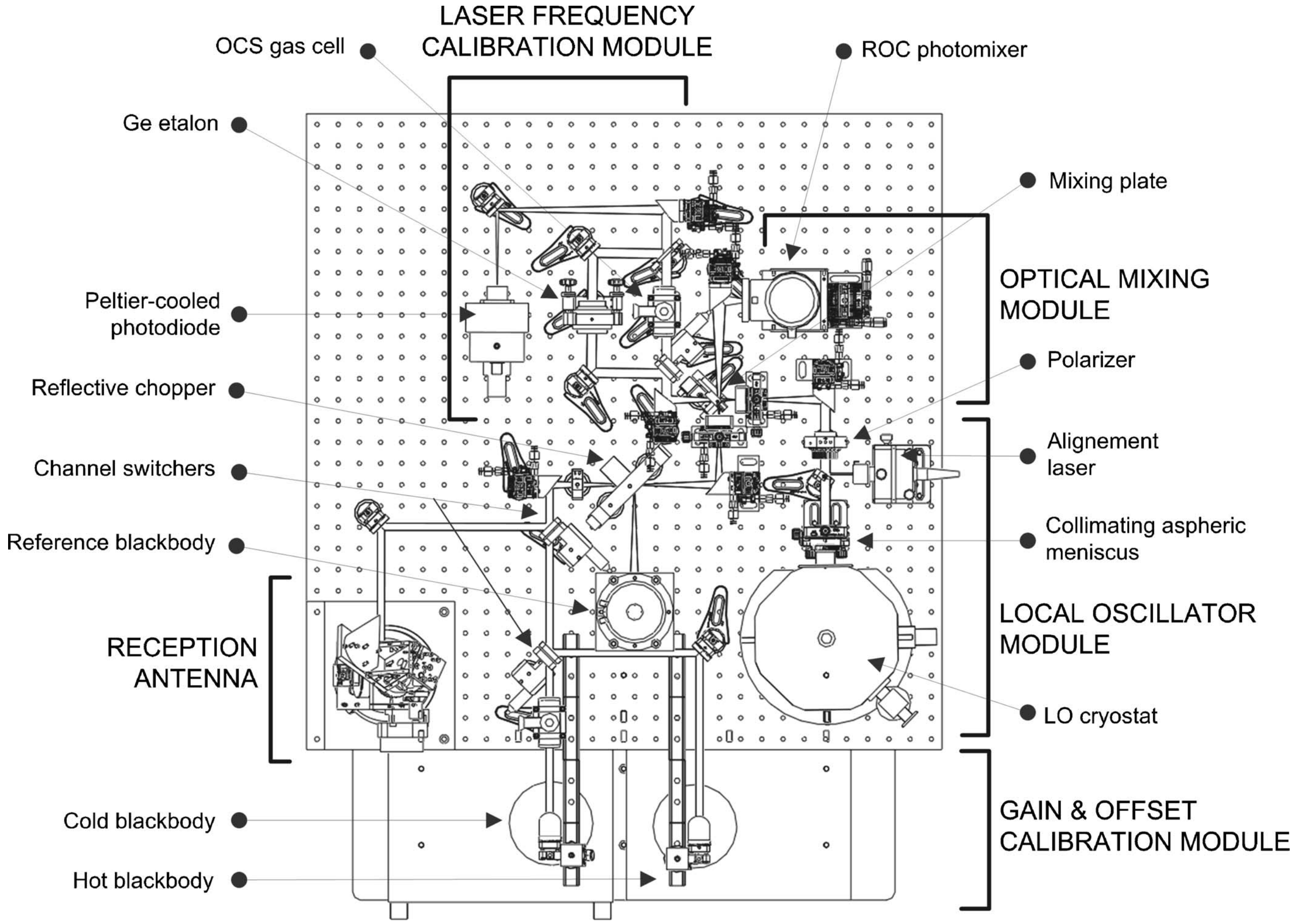

FIG. 3. Plan view of the instrument optical bench showing the optical setup. The different modules described in the text are indicated.

the photomixer and associated electronics. In the mid-IR (at 10 μm), matured photomixer technologies can offer double sideband bandwidth in the range of $\sim$4 GHz, which corresponds to an analyzed spectral microwindow of $\sim$0.013% of the central frequency. By using a 10 cm^{-1} continuously tunable LO, the spectral range increases to up to 1% of the central frequency. A wider spectral coverage makes the instrument potentially more useful, perhaps simultaneously measuring spectral features arising from several atmospheric species.

Tuning the LO frequency provides the following advantages:

– Elimination of IF analysis reduces complexity.
– The absolute requirement for a high-speed photomixer is relaxed.
– Active stabilization of LO frequency is not required.
– The instrument line shape (ILS) is defined by a single RF filter and is easy to characterize.

However, there are also some disadvantages that cannot be ignored:

– Optical feedback from spurious reflections from the photomixer is a major source of noise.
– The LO power varies during tuning, and this also effects the shot noise.
– The spectral multiplexing advantage is lost.

The ideal situation would be a system offering both capabilities by combining the use of a tunable LO and an IF frequency analyzer.

IV. INSTRUMENT DESIGN

The LHR was built on a portable workstation, which also housed all of the electronics. The workstation supports a 0.75×0.75 m^2 optical breadboard, which is mechanically decoupled from the rest of the structure by vibration dampers.

With the exception of the laser collimating meniscus the optical system is wholly achromatic. The exclusive use of reflective optics also reduces spurious reflections that can feed back into the laser and significantly limit the instrument's performance.[30] Off-axis reflective optics require careful alignment and this was achieved using an infrared imaging camera. These optical components may also introduce beam distortion.[31] However, these effects have been minimized by using relatively slow reflective optics ($>f/4$).

Figure 3 shows a plan view of the optical breadboard. For the sake of clarity, the instrument will be described as a series of submodules as they appear in Fig. 3.

A. Local oscillator module

A custom made liquid-nitrogen cryostat (Infrared Laboratories) houses the QCL. The cold finger is actively stabilized to ±0.5 mK by a temperature controller (Lakeshore, model 340). The QCL current is provided by a low-noise diode laser controller (ILX model LDC-3744B). The infrared beam exits the cryostat through a wedged barium fluoride window and is collimated by a 12.5 mm diameter $f/0.5$ ZnSe aspheric meniscus. For alignment purposes a visible diode laser beam may be introduced along the optical axis of the infrared radiation using a flip mirror. A barium fluoride wire-grid polarizer is used as a variable attenuator to regulate the local oscillator power.

B. Optical mixing module

The laser radiation is focused by a 101.6 mm focal length off-axis paraboloidal mirror (OAPM), creating an intermediate image of the QCL that is useful for beam manipulation and characterization. The LO beam is incident on a mixing plate, a ZnSe beam splitter ($R=25\%$, $T=75\%$), where it is superimposed with radiation from the scene. The reflected part of the LO radiation is focused on a high-speed HgCdTe photodiode by a 79.06 mm focal length off-axis ellipsoidal mirror (OAEM). The photodiode is circular with 100 μm diameter. It has a resonant optical cavity designed for peak sensitivity at 9.7 μm and an electrical bandwidth of up to 3 GHz. The dc part of the signal from the photomixer is used for alignment and power monitoring, whereas the high-frequency component (10 Mz–3 GHz) is amplified by two cascaded amplifiers with a gain of 30 dB each. Two different biasing and amplifying assemblies were used: one for signals with a bandwidth below 1 GHz, giving a 46% heterodyne efficiency, and the other for bandwidths of up to 3 GHz, providing 41% efficiency. 3 GHz is the instrument's lowest single sideband resolution. For a particular measurement, the receiver bandwidth and ILS can be tailored to give the optimal resolution using RF filters with a bandwidth between 5 MHz and 3 GHz.

A quarter-wave plate inserted in the beam before the photomixer, in combination with the polarizer in the LO module, provides 30 dB of optical isolation.[32] The efficiency of the isolation, with respect to the LO frequency sweeping has been described fully in Ref. 30.

C. Laser frequency calibration module

The LO radiation transmitted by the mixing plate is recollimated by a 101.6 mm OAPM. The laser radiation is directed to either a germanium etalon or a 5 cm long glass gas cell fitted with barium fluoride wedged windows before reaching a peltier-cooled HgCdZnTe photodiode (Vigo Systems). The Germanium etalon provides a relative frequency calibration with a free spectral range of 0.0485 cm^{-1}. The gas cell provides an absolute frequency reference; a few millibars of carbonyl sulphide were used during this work, with line positions taken from the high-resolution transmission molecular absorption (HITRAN) database.[33]

D. Gain and offset calibration module

Radiation sources are selected via motorized flipping mirrors. Two calibrated blackbody cavities (Isotech, models Gemini and Hyperion) each with an emissivity of better than 0.995 may be selected: a low-temperature cavity operating between 263 and 353 K and a high-temperature cavity operating in the range of 373–773 K. The radiation from these sources is collimated by 203.2 mm focal length OAPMs. A glass gas cell similar to the one used in frequency calibration module may be inserted into the optical path to perform heterodyne spectroscopy against the blackbody sources. Alternatively radiation collected by a receiving antenna may be selected. The antenna is composed of a 50 mm diameter OAPM and shaping optics mounted on a motorized equatorial mount.

The selected input beam is focused onto the blades of a reflective mechanical chopper by a 101.6 mm focal length OAPM. The incoming radiation may be modulated against a fixed reference provided by a liquid-nitrogen cooled blackbody. The optical image formed in the plane of the chopper blades is refocused by a 62.5 mm focal length OAEM and superimposed with the LO radiation at the mixing plate.

Two different optical filters were used: a ZnSe 8–12 μm band pass filter and a germanium long pass filter to remove visible wavelengths during solar occultation measurements.

E. Signal processing and acquisition

The core of the acquisition system is a digital signal processing (DSP) lock-in amplifier (Ametek model 7265). The RF signal power output by the photomixer and amplifiers is detected by a zero-bias Schottky diode (Herotek DZ401, 100 kHz–4 GHz bandwidth, 1200 mV/mW sensitivity). The resulting signal is fed into the lock-in amplifier for demodulation. The lock-in amplifier has three analog to digital converters used to acquire the dc signal from the photomixer and signals from the laser frequency calibration module. 8 bit digital output is also available and was used to control the state of the motorized mirror flipper mounts. An internal oscillator provides the synchronization signal controlling the mechanical chopper.

A general purpose interface bus (GPIB) interface is used to link the current source, the temperature controller, the lock-in amplifier, a waveform generator, and a digital oscilloscope to a laptop personal computer (PC) equipped with LABVIEW software. The blackbodies are controlled via a RS 232 interface.

LABVIEW software was developed to control the instrument in several operating modes and process recorded signals.

V. PRELIMINARY LABORATORY RESULTS

A. OCS absorption and emission

The $2\nu_2$ band of carbonyl sulfide (OCS) at 1047 cm^{-1} has strong absorption lines with intensities of the order of 10^{-21} cm^{-1}/molecule cm^{-2}. Unlike ozone OCS remains stable in absorption cells. For these reasons OCS was chosen to evaluate the LHR in the laboratory.

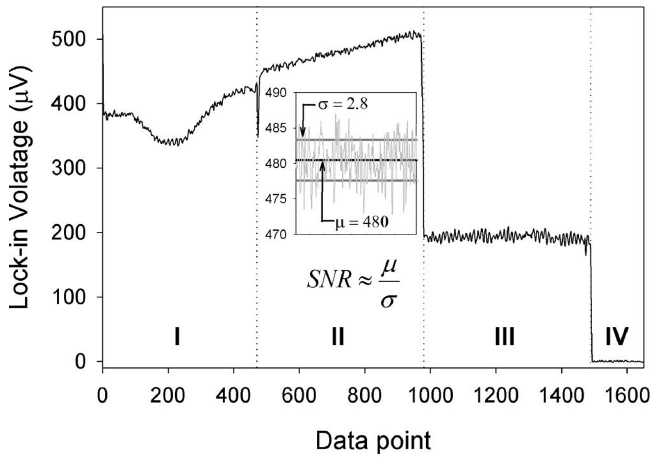

FIG. 4. The heterodyne signal recorded during laboratory measurements. The LO frequency was tuned by varying the QCL current. In sections I and II of the measurements the instrument was targeting a 373 K blackbody. A 5 cm long gas cell filled with 20 mbars, of OCS was placed in the optical path in section I. The cell was removed between sections I and II, and during section III the instrument viewed a blackbody at ambient temperature. The QCL is switched off during section IV. The inset in section II shows the base line corrected signal used to calculate an estimate of the signal-to-noise ratio.

A glass gas cell filled with 20 mbars of pure OCS was positioned in front of the hot blackbody source, with cavity set to 373 K. The QCL operating conditions were set to 96 K and 830 mA to target the P33 line of OCS at 1034.3261 cm^{-1}. The QCL current was swept over a range of 60 mA during a period of 500 s, resulting in a 0.24 cm^{-1} wide laser frequency scan. Four measurements were made in total and the recorded in-phase component of the demodulated signal is shown in Fig. 4. Two of the measurements viewed the blackbody; one with and one without the gas cell, corresponding to sections I and II in Fig. 4, respectively. A third measurement was made viewing an ambient blackbody target, corresponding to section III in Fig. 4. A final measurement was made with the QCL switched off, corresponding to section IV in Fig. 4. During these measurements the LO power was 0.5 mW, the integration time was 1 s and the equivalent double sideband detection bandwidth was 4 GHz. The 0–200 MHz frequency range was rejected to eliminate excess noise introduced by the LO (see details in Ref. 30). The modulation frequency was set to 1.8 kHz.

The shape of the OCS absorption line observed in section I of Fig. 4 results from a convolution of the ILS with the true absorption line shape (linewidth is 1.9 GHz). As the cell is removed from the optical path, a small change in signal occurs which is related to losses caused by the cell windows. Modulation of the LO power occurs with the change in current, and this is responsible for the observed base line variation. Ignoring the base line variation, the SNR calculated from section II is 171 (see inset in section II, Fig. 4) which is only a factor of 3 worse than the theoretical shot-noise limit. The SNR calculated from the data shown in section III of Fig. 4 is 31, and this corresponds to a received radiance equivalent to a 265 K blackbody emitter.

By sweeping the QCL operating temperature a wider spectral range can be scanned than by current tuning. Temperature tuning has the advantage that the QCL slope efficiency is unaffected thus reducing the optical power modulation associated to the frequency scan. In heterodyne systems there is no requirement for the fast scanning that is possible with current tuning because integration times must necessarily be long. Two current tuning methods were compared: a single slow scan with a long integration time (1 s) and repeated fast scans (10 ms integration time). For identical total measurement times there were not any significant differences between the two methods in terms of SNR.

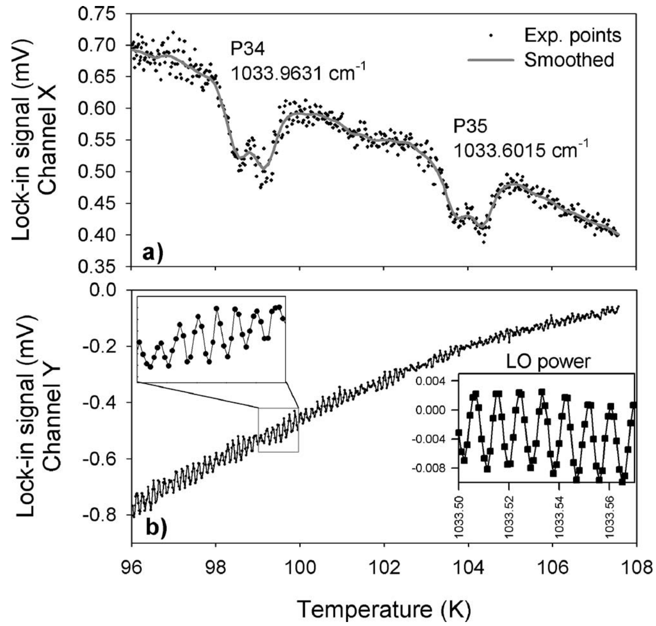

FIG. 5. (a) In-phase heterodyne signal during temperature tuning of the LO frequency across two OCS absorption lines. The smoothed line is obtained by low pass filtering. The background was a 373 K blackbody. (b) Corresponding quadrature signal. The enlarged section (left) shows residual etalon fringes and the inset panel shows the corresponding relative variation in LO power.

Figure 5 shows the heterodyne signal observed when an absorption cell, this time filled with 55.7 mbars of pure OCS, was placed in front of a 373 K blackbody. The laser current was set at a constant 850 mA and the temperature was increased from 96 to 108 K at a rate of 0.5 K/min. Photomixer amplifiers were configured with a 1 GHz bandwidth. Integration time was set to 1 s. Since the spectrum is over-

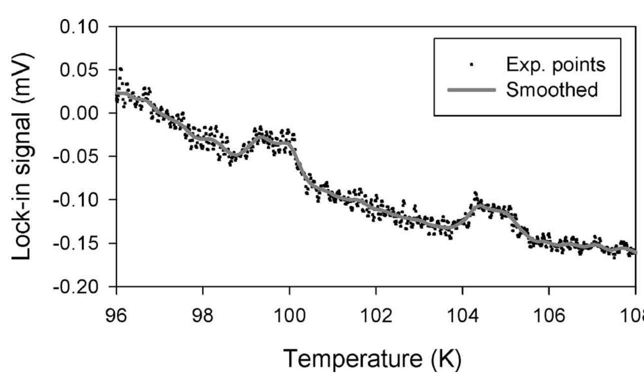

FIG. 6. OCS spectrum recorded under the same conditions as that in Fig. 5 but using a 263 K blackbody. In this case the OCS emission is greater than the background and the heterodyne radiometer resolves an OCS emission spectrum.

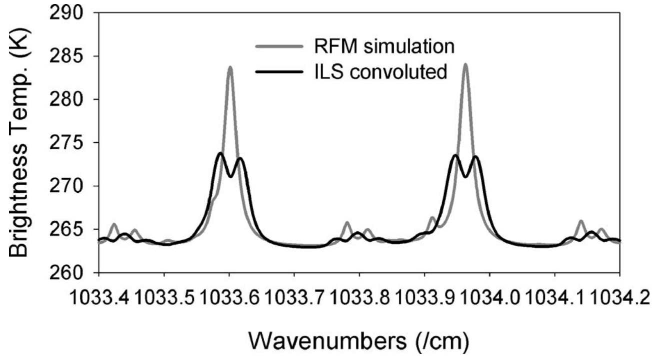

FIG. 7. Calculated OCS emission spectrum corresponding to the experimental conditions of Fig. 6. The base line variation due to the LO power modulation was not included in the model.

sampled an additional low pass filtering has been applied to the data (solid line). The base line exhibits a negative slope consistent with LO power modulation with increasing laser operating temperature. The central dip appearing on the OCS P35 and P34 lines is an artifact of the ILS, which can be considered as a boxcar function spanning the ±1 GHz range with a 400 MHz wide rectangular dip in the center. A variation in the noise level with LO temperature is noticeable in both the in-phase signal (channel X) shown in Fig. 5(a) and the quadrature signal (channel Y) shown in Fig. 5(b). To obtain the signals in the X and Y channels a phase rotation was applied until any spectral information was suppressed in the Y channel. This residual noise is introduced by a spurious reflection, and the corresponding cavity length has been found to match the distance between the QCL and the photomixer (~54 cm). The variation in fringe contrast as the laser frequency is changed indicates that the optical isolation efficiency varies with frequency. Indeed the retardation introduced by the quarter-wave plate is a function of frequency. The inset panel in Fig. 5(b) shows the corresponding relative variation in dc power as measured by the photomixer.

To further investigate the capabilities of the instrument spectroscopic measurements were made in emission. This time the OCS cell was introduced in the optical path of the cold blackbody set at a temperature of 263 K. As previously the laser wavelength was scanned by varying temperature. All other experimental conditions were identical except the integration time, which was increased to 2 s. The observed spectrum is shown in Fig. 6. In this configuration the emission from the OCS molecules was greater than the background. The corresponding calculated spectrum [using the reference forward model[34] (RFM)] is shown in Fig. 7. The true spectrum and the convolution of the spectrum with the ILS are shown. This confirms that the instrument could be used for measuring atmospheric ozone emission from the ground at low elevation angles and demonstrates that it is also suitable for limb sounding and nadir sounding from space. This will be discussed in a future publication.

As infrared heterodyne receivers are primarily intended to be used at long integration times, it is interesting to investigate temporal stability through Allan variance analysis.[35] The LHR was set to observe the 373 K blackbody at fixed LO frequency for a period of 24 min and a 1 s integration time. The bandwidth was set to 220 MHz with a band pass filter. The Allan variance of the recorded signal was calculated,[36] and the results are shown in Fig. 8(a). Thus no real improvement in SNR should be expected for integration times longer than 10 s. This limitation in stability was traced to an unexpectedly unstable LO power level at the photomixer. Figure 8(b) shows the Allan variance plot of the corresponding LO power signal; an identical 10 s rollover time was observed. The negative slope before the rollover in Fig. 8(a) is not equal to −1 as expected from a signal only affected by white noise. Additional excess noise coming from the QCL is expected to be still present since the RF filters used in the study did not reject the entire low-frequency laser noise completely.[30]

The lack of stability is due to the highly critical alignment tolerance of the collimating aspheric meniscus. The meniscus is a very fast optic, and the QCL beam waist at the chip output facet is ~5 μm in its smallest dimension. Hence, the slightest misalignment results in a degradation of the LO image at the photomixer. Spectacular drops in LO power could be observed as rays of sunlight shone onto the optical table, causing thermal variations in the optical mount of the meniscus.

VI. ATMOSPHERIC MEASUREMENT CAMPAIGN

The LHR was located in a south-facing laboratory at the Rutherford Appleton Laboratory (position 51:34:17N, 1:18:53W and 110 m above sea level) to perform solar occultation measurements on atmospheric ozone. All of the measurements reported here were made on 21 September 2006 between 10:00 and 12:30 UT.

All spectra were obtained by temperature tuning of the LO frequency. Examples of atmospheric transmission spectra covering up to a 2 cm^{-1} spectral range are shown in Fig. 9. Table I summarizes the experimental parameters relevant to each of the spectra appearing in Fig. 9, which were all recorded with a 0.5 s integration time and a 220 MHz double sideband bandwidth. Each spectral plot includes a theoreti-

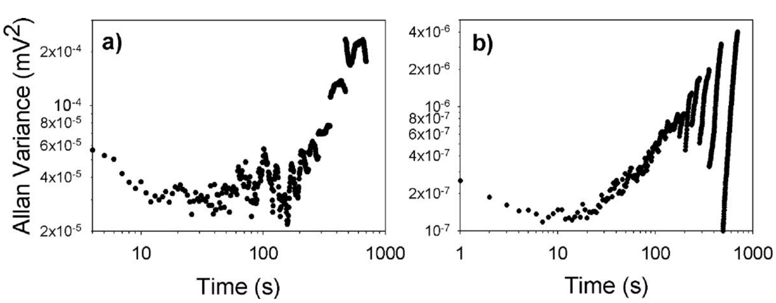

FIG. 8. Allan variance calculations for (a) the heterodyne signal and (b) the LO power signal. Both plots show a rollover at around 10 s.

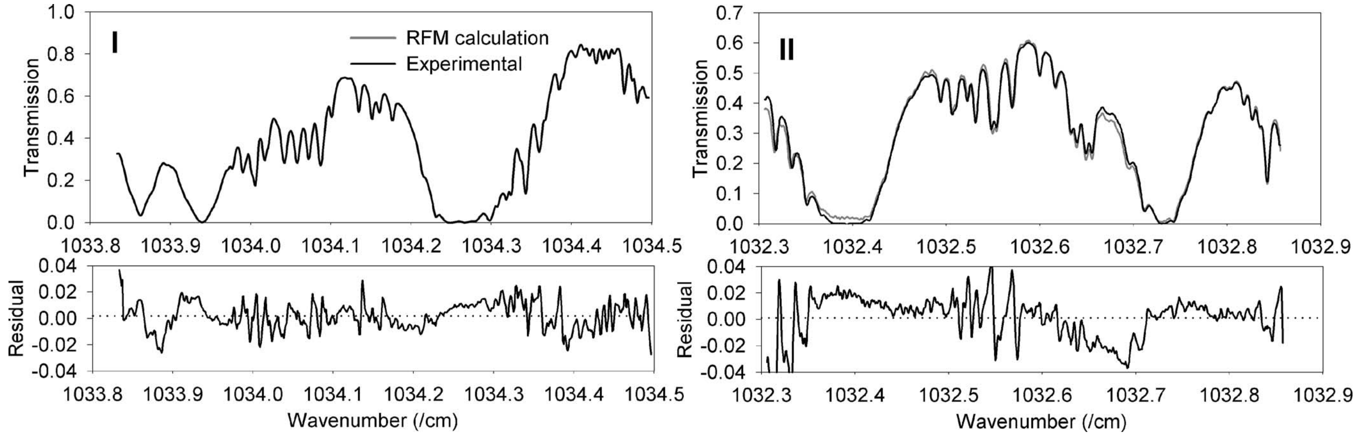

FIG. 9. Atmospheric transmission spectra obtained with the QCL-based LHR operating in solar occultation mode. Experimental and calculated spectra are shown, as well as the corresponding residuals.

cally calculated spectrum derived using the RFM, the HITRAN 2004, database and a typical mid-latitude daytime atmospheric profile. Below each graph, the corresponding residual transmission is shown. Note that no fitting of the atmospheric profiles was performed at this stage. However, the raw spectra have been corrected to account for a base line variation using a fitting procedure. The variation of the local oscillator power, the slight misalignment of the main collection antenna, and the potential partial obscuration of the FoV by thin subvisible clouds contribute to the base line variation with time. Corrections were made using a third order polynomial. In the future LO power variation and solar irradiance variation will be accurately measured and included in the forward model. The main residual features come from a slight mismatch in the frequency scales, generating "derivative-like" residuals. A more sophisticated frequency calibration will be investigated in the future. Other discrepancies are related to the use of the standard atmospheric profile, absorption features from species which are not included in the model, or from transitions which are not archived in the HITRAN 2004 database. As a whole, the majority of the absorption lines in this spectral region are due to ozone absorption, and at first glance the line broadenings indicate both stratospheric and tropospheric contributions. A procedure to optimally retrieve the ozone concentration profile information contained in the spectra is currently under development.

VII. DISCUSSION

The performance of the prototype quantum cascade laser heterodyne radiometer was found to be excellent: the best results indicated a detection limit of only three times the theoretical shot-noise limit. The capabilities of the instrument have been demonstrated through absorption and emission spectroscopy in the laboratory, as well atmospheric measurements. This study has identified the main factors limiting the instrument performance during routine operation:

– Excess noise from the LO in the 0–200 MHz range. Although the rejection of this band should minimize impact on atmospheric profile retrievals, a cleaner LO would be beneficial.
– Optical feedback from the photomixer. A 30 dB isolation system based on a quarter-wave plate has been implemented, which has efficiently reduced feedback. Increased isolation from a dedicated Faraday rotator would further reduce optical feedback.
– Mechanical instability in the collimating meniscus generated unexpected LO power variations and limited the stability of the radiometer. This problem can be overcome using improved optical mounting systems and by shielding the instrument from thermal variations.

Atmospheric transmission spectra covering a 2 cm^{-1} spectral range were recorded. The laser was not pushed to its limits during the study and an additional 2 cm^{-1} tuning range is possible. Work is currently in progress to retrieve vertical profile information on ozone concentration from the atmospheric spectra. Two-dimensional (wave number and LO power) gain and offset calibration tables will provide direct measurements in brightness temperature.

This successful demonstration of the LHR in a LO frequency sweeping mode opens the path to compact, lightweight, and optically integrated IR heterodyne systems with

TABLE I. Summary of experimental parameters during field observations on 21 September 2006, corresponding to spectra in Fig. 9

Spectrum	QCL current (mA)	Tempertural scan (K)	Scan rate (K/min)	Tuning rate (cm^{-1}/K)	Tuning offset (cm^{-1})	Sun elevation (°)	Time (UT)
I	800	96 → 106	1	−0.0664	1040.8752	36.38	10:38
II	900	105 → 115	0.5	−0.0684	1040.3772	39.05	12:08

no moving parts. Such systems would be potential candidates for deployment on high altitude or satellite platforms. The results obtained with the ground-based prototype instrument are being used to predict the likely performance of an aircraft or space based instrument.

ACKNOWLEDGMENTS

The authors wish to thank colleagues within the Space Science and Technology Department of the Rutherford Appleton Laboratory: Gary Williams and Brian Landowsky for their technical assistance and also Dr. Richard Siddans for his assistance during laser wavelength selection. Dr. William Bell from the UK Meteorological Office is also acknowledged for useful discussions. This work was supported by the Natural Environment Research Council (Grant No. NER/Z/S/2003/00642).

[1] M. C. Teich, R. J. Keyes, and R. H. Kingston, Appl. Phys. Lett. **9**, 357 (1966).
[2] R. T. Menzies and M. S. Shumate, Science **184**, 570 (1974).
[3] R. T. Menzies, in *Laser Monitoring of the Atmosphere* edited by E. D. Hinkley (Springer, Berlin, 1976), Chap. 7.
[4] K. E. Fast, T. Kostiuk, F. Espenak, T. A. Livengood, T. Hewagama, and M. F. A'Hearn, Geophys. Res. Lett. **31**, L08109 (2004).
[5] W. Bell, N. A. Martin, T. D. Gardiner, N. R. Swann, P. T. Woods, P. F. Fogal, and J. W. Waters, Geophys. Res. Lett. **21**, 1347 (1994).
[6] T. Kostiuk, International Thermal Detectors Workshop, 19–20 June 2003 Session 7 (unpublished).
[7] T. Kostiuk, Infrared Phys. Technol. **35**, 243 (1994).
[8] T. Kostiuk *et al.*, Geophys. Res. Lett. **32**, L22205 (2005).
[9] M. J. Mumma, D. Buhl, G. Chin, D. Deming, F. Espenak, T. Kostiuk, and D. Zipoy, Science **212**, 45 (1981).
[10] C. H. Townes *et al.*, Proc. SPIE **3350**, 908 (1998).
[11] G. Sonnabend, D. Wirtz, F. Schmulling, and R. Schieder, Appl. Opt. **41**, 2978 (2002).
[12] D. Weidmann and D. Courtois, Appl. Opt. **42**, 1115 (2003).
[13] J. Faist, F. Capasso, D. L. Sivco, C. Sirtori, A. L. Hutchinson, and A. Y. Cho, Science **264**, 553 (1994).
[14] T. Aellen, S. Blaser, M. Beck, D. Hofstetter, J. Faist, and E. Gini, Appl. Phys. Lett. **83**, 1929 (2003).
[15] R. Maulini, M. Beck, J. Faist, and E. Gini, Appl. Phys. Lett. **84**, 1659 (2004).
[16] G. Sonnabend, D. Wirtz, and R. Schieder, Appl. Opt. **44**, 7170 (2005).
[17] G. Sonnabend, D. Wirtz, V. Vetterle, and R. Schieder, Astron. Astrophys. **435**, 1181 (2005).
[18] G. Sonnabend, M. Sornig, P. J. Krötz, R. T. Schieder, and K. E. Fast, Geophys. Res. Lett. **33**, L18201 (2006).
[19] M. A. Frerking and D. J. Muehlner, Appl. Opt. **16**, 526 (1977).
[20] M. M. Abbas, T. Kostiuk, M. J. Mumma, D. Buhl, V. G. Kunde, and L. W. Brown, Geophys. Res. Lett. **5**, 317 (1978).
[21] H. Fukunishi, S. Okano, M. Tagushi, and T. Ohnuma, Appl. Opt. **29**, 2722 (1990).
[22] J. C. Mouanda, A. Hamdouni, D. Courtois, and C. Thiébeaux, Infrared Phys. Technol. **37**, 575 (1996).
[23] K. Rohlfs, *Tools of Radioastronomy* (Springer, Berlin, 2004).
[24] P. R. Griffiths and J. A. de Haseth, Fourier Transform Infrared Spectrometry (Wiley, New York, 1986).
[25] F. Schmülling, B. Klumb, M. Harter, R. Schieder, B. Vowinkel, and G. Winnewisser, Appl. Opt. **37**, 5771 (1998).
[26] D. Weidmann and D. Courtois, J. Quant. Spectrosc. Radiat. Transf. **83**, 655 (2004).
[27] T. Kostiuk and D. L. Spears, Int. J. Infrared Millim. Waves **8**, 1269 (1987).
[28] W. J. Reburn *et al.*, ESA Contract No. 13348/98/NL/GD, final report, 2000 (unpublished).
[29] C. Rodgers, *Inverse Methods for Atmospheric Sounding: Theory and Practice* (World Scientific Publishing, 2000).
[30] D. Weidmann, K. Smith, and B. Ellison, Appl. Opt. **46**, 947 (2007).
[31] P. F. Goldsmith, *Quasioptical Systems* (IEEE, New York, 1998), Chap. 5.
[32] R. Schieder, Infrared Phys. Technol. **35**, 477 (1994).
[33] L. S. Rothman *et al.*, J. Quant. Spectrosc. Radiat. Transf. **96**, 139 (2005).
[34] A. Dudhia, "Reference forward model software user's manual," ww.atm.ox.ac.uk/RFM/sum.
[35] R. Schieder and C. Kramer, Astron. Astrophys. **373**, 746 (2001).
[36] T. J. Witt, IEEE Trans. Instrum. Meas. **50**, 445 (2001).